# Propane/Propylene Diffusion in Zeolites: Framework Dynamics

**ARTICLE** *in* THE JOURNAL OF PHYSICAL CHEMISTRY C · JUNE 2009

Impact Factor: 4.77 · DOI: 10.1021/jp903245j



**2 AUTHORS:**

Aldo Fabrizzio Combariza Montañez
Universidad de Sucre
**19** PUBLICATIONS **96** CITATIONS
SEE PROFILE

German Sastre
Research Scientist
**118** PUBLICATIONS **2,365** CITATIONS
SEE PROFILE

# Propane/Propylene Diffusion in Zeolites: Framework Dynamics

**Aldo F. Combariza, German Sastre,* and Avelino Corma**

*Instituto de Tecnología Química, UPV-CSIC, Av/Los Naranjos s/n, 46022 Valencia, Spain*

*Received: April 8, 2009; Revised Manuscript Received: May 18, 2009*

Pure silica zeolites with narrow eight-membered (8-MR) oxygen rings are good candidates for separations of olefin/paraffin mixtures based on molecular sieving effects. We have used a molecular dynamics technique to study the structural features of two pure silica 8-MR frameworks: Si-CHA and Si-SAS. CHA and SAS are framework types with 3- and 1-dimensional porous systems, respectively, with cages connected through 8-MR windows. Window size temperature fluctuations were studied from equilibrium molecular dynamics simulations by allowing full flexibility of the framework. The thermal influence on diffusional features of propane/propylene molecules adsorbed in Si-CHA and Si-SAS zeolites is studied using classical molecular dynamics simulations. Potential energy surface effects are taken into account by comparing the results from the well-known van Beest, Kramer, and van Santen potential [*Phys. Rev. Lett.* **1990**, *64*, 1995] and the Pedone, Malavasi, Menziani, Cormack, and Segre potential [*J. Phys. Chem. B* **2006**, *24*, 11780].

## Introduction

Zeolites are microporous crystalline materials extensively used in a wide set of industrial applications due to their special characteristics such as large free volume, low density, void spaces in the form of cages and channels, thermal stability, and acid/base properties.[1] Catalysis, adsorption,[2] ion exchange, electronics,[3] molecular sieving, and many other interesting applications are now common fields of application for these materials. Separation of olefin/paraffin mixtures (ethene/ethane, propene/propane, butene/butane) is at the center of the scene due to the always growing demand of pure raw materials and the high level of energetic consumption involved in the separation process.[4] Separation of olefin/paraffin mixtures based on ionic exchanged zeolites is accomplished through $\pi$-complexation with Cu or Ag ions exchanged in the zeolite framework,[5,6] whereas in the case of pure silica zeolites the separation occurs as a consequence of a molecular sieving effect. In this regard, zeolites with windows formed by eight $SiO_4$ tetrahedral units (eight-membered ring, 8-MR) have been recognized as potential candidates for the specific separation of propylene/propane mixtures.[7] However, slow diffusivity in these systems, which arises as a consequence of the close match between guest kinetic diameter and window size, makes experimental determination of diffusivities a difficult task and also challenges computational methods such as molecular dynamics (MD) to make estimates in computer-accessible time scales. Nevertheless, MD is the method of choice to study diffusion because it provides atomistic information of the dynamics of every particle of the system, which can be easily related to experimental measurements.

In this work we investigate the framework dynamics and the diffusion of propane and propene adsorbed in two pure silica 8-MR zeolites using an MD technique. Computational studies on 8-MR zeolites have focused on the dynamics of guest molecules while ignoring the flexibility of the host,[8] although the framework flexibility is recognized to be an important factor when studying the diffusional behavior in host−guest systems, especially in tight-fitting systems.[9,10] Our approach is based on the fact that intracrystalline motion through 8-MR windows present in zeolites regarded as candidates for propane/propene separation is critically controlled by the dimensions of the window. In the case of propylene/propane adsorbed in 8-MR zeolites, the window size is a critical property due to the size of the guest kinetic diameter, which closely matches the size of the window aperture. Thus, the main objective of this work was to study the dynamical structural features, specifically the temperature influence on window sizes and fluctuations of two 8-MR all-silica zeolites, and the intracrystalline diffusion of two hydrocarbons (propylene/propane) whose kinetic diameter matches closely the 8-MR aperture.

Experimentally it has been found that negative thermal expansion commonly occurs in low-density microporous materials, as in the case of zeolites.[11,12] This negative thermal expansion will have an effect upon the window dimensions of the frameworks and therefore should be a factor to include when applying computational techniques to simulate the dynamics of host−guest systems. From this starting point, an MD procedure was developed to account for the change in the cell volume with temperature. Thermal dependence of the 8-MR structure and diffusion was investigated by running simulations at different temperatures. The influence of the force field (FF) was also accounted for by comparing the results from two FFs: the van Beest, Kramer, and van Santen (BKS) force field[13] and the Pedone, Malavasi, Menziani, Cormack, and Segre (PMM) partial charge potential.[14] The BKS FF[13] was our first choice to represent the zeolite structure because of its ability to accurately reproduce structural features of silica-containing materials, although the limitations of the model in representing the vibrational density of states (VDOS) are well documented.[15] The PMM partial charge potential uses a Morse function to describe the short-range ionic interactions. It has been parametrized with experimental structural information on a series of oxides, and parameters are provided for silica-containing materials. As the BKS and PMM FFs are based on different functional forms representing the nonbonded Si−O interactions, we expect to magnify the influence of the FF by highlighting the structural and diffusional features of the host−guest systems

* To whom correspondence should be addressed. E-mail: gsastre@itq.upv.es.

10.1021/jp903245j CCC: $40.75 
Published on Web 06/09/2009

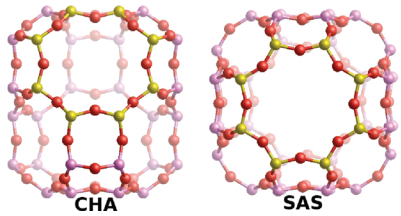


**Figure 1.** CHA and SAS cages.

**TABLE 1: Pure Silica CHA and SAS Zeolites: Lattice Parameters and Cell Volume**

| zeolite | *a* (Å) | *b* (Å) | *c* (Å) | α (deg) | *β* (deg) | *γ* (deg) | vol (Å$^3$) |
|---|---|---|---|---|---|---|---|
| SSS-73[16] | 14.104 | 14.104 | 10.187 | 90.00 | 90.00 | 90.00 | 2026.50 |
| Si-CHA[17] | 13.675 | 13.675 | 14.767 | 90.00 | 90.00 | 120.00 | 2391.54 |

predicted with the different FFs. The selected FFs were also chosen on the basis of features related to computational processing time and implementation complexity.

The remainder of this paper is as follows: In Models we describe the pure Si zeolite structures chosen. In Methods we state the details of the molecular dynamics methods used, specifically the functional forms used to represent the potential energy surface of the systems and the algorithms used to analyze the information obtained from the simulations. The Results and Discussion presents the results on the structural dynamics of the frameworks and the diffusion parameters obtained, followed by the discussion and analysis of the results. Concluding remarks and proposed further work will be stated in the Conclusion.

## Models

We have selected two pure silica framework types, namely, Si-SAS and Si-CHA. The pure silica SAS framework type, or zeolite SSZ-73, is a 1-dimensional channel structure formed by eight, six, and four ring units, with *I*4/*mmm* space group symmetry.[16] SSZ-73 is unusual in that it is 1-dimensional with small pores, yet has a very large micropore volume due to its sizable cages. SSZ-73 has a nitrogen micropore volume of 0.25 cm$^3$/g, which is surprisingly high for a 1-dimensional molecular sieve. SSZ-73 also has an unexpectedly high surface area of about 585 m$^2$/g. Pure silica CHA has a rhombohedral unit cell containing 36 atoms, with space group symmetry *R*3*m* and with four crystallographic distinct Si−O−Si angles.[17] It is formed by rings of eight, six, and four members in a 3-dimensional network of interconnected cages (see Figure 1). Table 1 shows the lattice parameters and volumes of the selected zeolite structures.

## Methods

**Molecular Dynamics Technique.** MD simulations are carried out to simulate the diffusion of either propane or propylene molecules in two pure silica framework types using the parallel general purpose DL_POLY_2.20 code.[18] We have included full framework/guest flexibility in our approach, as framework flexibility has been recognized to have a big impact on the diffusional behavior of adsorbates in nanoporous materials. Our strategy also takes into account the temperature influence on the systems. This is because changes in cell size with temperature will add at least two factors to the diffusional behavior of the guest through host channels/pores: changes in cell volume would change 8-MR window sizes and thus the ability of guest molecules for intercage window-crossing motion, and as the mobility of guest molecules is affected by changes in temperature, it would also exert an influence from a thermally activated diffusion point of view.[12]

**TABLE 2: Force Field Parameters**

| | BKS | | PMM | |
|---|---|---|---|---|
| charge (e) | | | | |
| $Si_c$ | +2.4 | | +2.4 | |
| $O_c$ | −1.2 | | −1.2 | |
| | Buckingham (eq 7) | | Morse (eq 8) | |
| | $A_{Si-O}$ (eV) | 18003.7572 | $D_e$ (eV) | 0.340554 |
| | $A_{O-O}$ (eV) | 1388.7730 | $a_{Si-O}$ (Å$^{-2}$) | 2.006700 |
| | $\rho_{Si-O}$ (Å) | 0.205205 | $r_{Si-0}$ (Å) | 2.100000 |
| | $\rho_{O-O}$ (Å) | 0.362319 | $D_e$ (eV) | 0.042395 |
| | $C_{Si-O}$ (eV Å$^6$) | 133.5381 | $a_{O-O}$ (Å$^{-2}$) | 1.379316 |
| | $C_{O-O}$ (eV Å$^6$) | 175.0000 | $r_{O-O}$ (Å) | 3.618701 |

Simulation cells are obtained from experimental positions of the unit cell followed by a 2 × 2 × 2 scaling of the unit cell. The velocity-Verlet algorithm is used throughout to integrate Newton's equations of motion with a time step of 1 fs. The loading was set to 4 guest molecules for both simulation cells, corresponding to 0.5 molecule per unit cell, with Si-CHA and Si-SAS unit cells containing 36 and 32 $SiO_{4/2}$ tetrahedral units, respectively. This low loading was chosen to ensure that intra/intercage mobility is not controlled by adsorbate−adsorbate interactions. Systems sampling either the NPT or NVE ensemble were simulated at 300, 400, 600, and 800 K.

Simulations start by assigning initial velocities from a Maxwell−Boltzmann distribution to the system atoms and allowing a pre-equilibration period of 10 ps in which velocities are updated every 10 steps until reaching the required target temperature. A second equilibration is then initiated by sampling the NPT phase space for at least 200 ps or after volume stabilization of the simulation cell is achieved. This equilibration in the NPT ensemble is essential if volume cell changes with temperature are to be accounted for. The Berendsen thermostat and barostat were used to control temperature and pressure at this step. Configurations matching the average volume cell are then sampled and stored for the next step.

After the NPT volume equilibration procedure, the sampled configurations are used as initial points for trajectories under the NVE ensemble. These runs are initiated by an equilibration of 20 ps, in which the velocities are scaled every 10 fs to the target temperature. Production runs are then allowed to run up to 12 ns. Analysis of the trajectories is then carried out from the history files generated. Two analysis tools are used: mean square displacements (MSDs) and pair distribution functions (PDFs). MSDs are calculated using the relationship

$$\langle X(t)^2 \rangle = \frac{1}{N_m N_{t_0}} \sum_{N_m} \sum_{t_0} [X_i(t + t_0) - X_i(t)]^2 \qquad (1)$$

where $N_m$ is the number of guest molecules, $N_{t_0}$ is the number of time origins used for the average calculation, and $X_i$ is the coordinate of the center of mass of molecule *i*. PDFs are calculated according to

$$G(r)_{ab} = \frac{1}{G_{ab}} \left[ \frac{dN_{ab}}{dV} \right] \qquad (2)$$

where $N_{ab}$ is the average number of a−b pairs with distance between *r* and *r* + d*r*, $G_{ab}$ is the density of molecules a and b, and *V* is the volume of the system.

Self-diffusion constants were obtained from the Einstein relationship

$$2tD = \frac{1}{N_t}\langle \mathbf{r}(t + t_0) - \mathbf{r}(t)\rangle \quad (3)$$

where $\mathbf{r}$ is the guest center of mass position vector, $N_t$ is the number of translational degrees of freedom of the guest molecule, and the symbol $\langle\rangle$ denotes an ensemble average. From the self-diffusion coefficients obtained at the different temperatures it is possible to estimate the Arrhenius activation energy from the following relation:

$$D = D_0 \exp\left[-\frac{E_a}{RT}\right] \quad (4)$$

where $R$ is the gas constant, $T$ is the temperature, and $E_a$ is the activation energy.

**Potential Energy Surface.** The potential energy surface (PES) of the system takes into account three main terms, the zeolite potential energy, $V^{zeo}$, the guest potential energy, $V^{guest}$, and the interatomic potential energy contribution, $V^{zeo-guest/guest-guest}$:

$$V^{total} = V^{zeo} + V^{guest} + V^{zeo-guest/guest-guest} \quad (5)$$

***Framework Potential.*** The PES of the framework was represented with a Coulombic part accounting for the long-range electrostatic interactions and a short-range two-body function which models the repulsion and the dispersion energy between close pairs:

$$V^{zeo} = V^{zeo\text{-}short} + V^{Coul} \quad (6)$$

To evaluate the Coulomb sum, we have used the particle mesh Ewald formalism,[19] as included in the DL_POLY code. We have chosen two different models for representing the short-range interactions of the selected pure silica materials under scrutiny. The first one is the well-known Born−Mayer model for ionic solids of van Beest et al. (BKS),[13] and the second corresponds to the Pedone et al.[14] (PMM) potential. The BKS potential is applied to oxygen−oxygen and oxygen−silica pair interactions. This potential (see eq 7) is divided into two terms: a repulsive contribution, given by the exponential term, and an attractive-dispersive one. This formulation allows a treatment of the interactions among the atoms as simple and physically reasonable as possible, for both short- and medium-range distances.

$$V_{BKS}^{zeo\text{-}short} = A_{ij} \exp\left(\frac{-r_{ij}}{\rho_{ij}}\right) - \frac{C_{ij}}{r^6} \quad (7)$$

The PMM model uses a Morse function to describe the short-range ionic interactions, although this function is normally used to describe bonding in organic covalent systems. In the application of the PMM potential, the Morse function is not used to describe a physically meaningful interaction, such as the dissociation energies or equilibrium bond distances, given by $D_{ij}$ and $r_{ij}$ in eq 8, respectively, but these parameters must be considered merely fitting parameters.[14]

$$V_{PMM}^{zeo\text{-}short} = D_{ij}\{[1 - \exp(a_{ij}(r - r_0))]^2 - 1\} \quad (8)$$

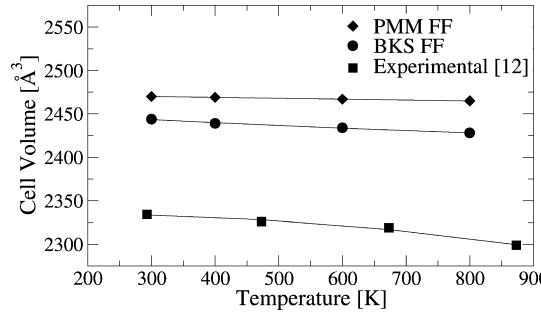


**Figure 2.** Evolution of experimental and calculated (BKS and PMM) cell volumes for Si-CHA in the range 300−800 K. Experimental values were taken from ref 12.

We refer the reader to the original references for in-depth information about the FFs. Parameters are presented in Table 2 for both FFs.

***Guest Potential.*** The potential for the hydrocarbons comprises two-body (bond), three-body (angle), and four-body (dihedral) interactions plus the electrostatic Coulomb term:

$$V^{guest} = V^{2B} + V^{3B} + V^{torsion} + V^{Coul} \quad (9)$$

$$V^{2B} = \frac{1}{2}k_{2B}(r_{ij} - r_{ij}^0)^2 \quad (10)$$

$$V^{3B} = \frac{1}{2}k_{3B}(\theta_{ij} - \theta_{ij}^0)^2 \quad (11)$$

$$V^{torsion} = k_{4B}[1 + \cos(n\phi_{ijk} - \phi_{ijk}^0)] \quad (12)$$

Parameters are given in the original reference by Oie et al.[20]

Finally, Lennard-Jones (LJ) potentials are used to describe the intermolecular, host−guest, energy interactions. The following 12−6 LJ functional form was used:

$$V^{zeo-guest/guest-guest} = 4\varepsilon_{ij}\left[\left(\frac{\sigma_{ij}}{r_{ij}}\right)^{12} - \left(\frac{\sigma_{ij}}{r_{ij}}\right)^{6}\right] + V^{Coul} \quad (13)$$

where $\varepsilon_{ij}$ is the well depth, $\sigma_{ij}$ is the diameter, and $r_{ij}$ is the distance between interacting particles $i$ and $j$. For a full set of parameters and a deeper description of the potential we refer the reader to the original references (refs 21 and 22).

## Results and Discussion

**Structural Dynamics of Si-CHA and Si-SAS.** We have first studied how Si-CHA and Si-SAS window sizes change with temperature. The experimental unit cell volume of Si-CHA reported by Hedin et al.[23] is 2348 Å$^3$ at 298 K and 101.3 kPa, and at similar conditions Woodcock et al.[12] reported a lower value of 2334 Å$^3$. The cell volume obtained from our MD simulations at 300 K with the BKS FF is 2442 Å$^3$, which is within 5% of the experimental values. The PMM cell volumes obtained are larger than the BKS ones. Figure 2 compares the cell volume calculated with the BKS and PMM FFs and the experimental results of Woodcock et al.

Experimentally it was found that the volume variation of Si-CHA is a nonlinear function of temperature, as can be seen in Figure 2. The temperature cell variation calculated with the BKS

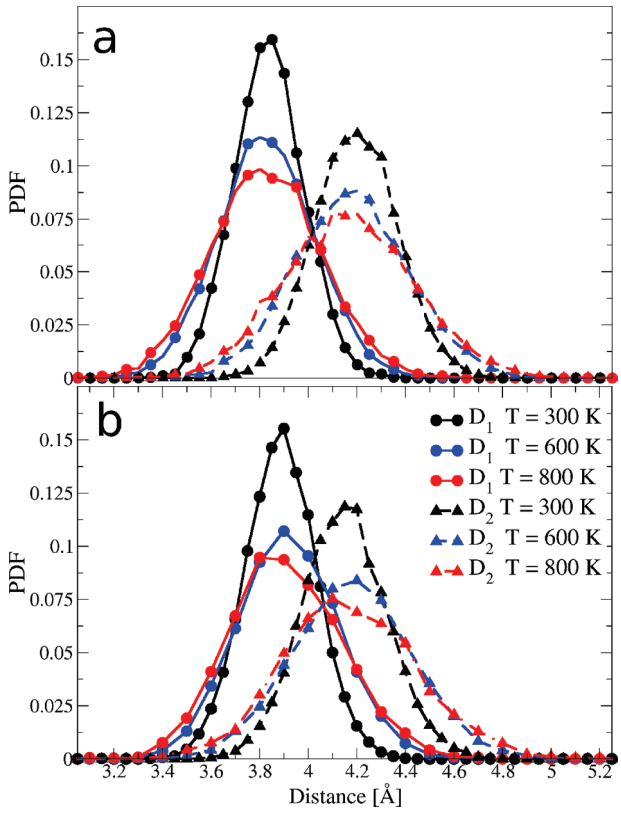


**Figure 3.** PDFs for 8-MR O−O distances $D_1$ and $D_2$ in Si-CHA obtained from MD trajectories at 300, 600, and 800 K using the BKS (a) and PMM (b) potentials.

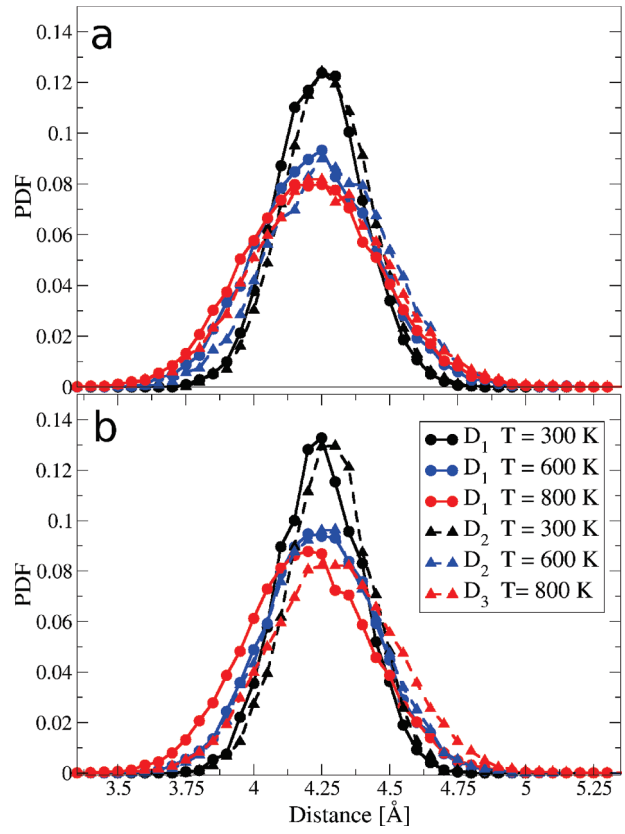


**Figure 4.** PDFs for 8-MR O−O distances $D_1$ and $D_2$ in Si-SAS obtained from MD trajectories at 300, 600, and 800 K using the BKS (a) and PMM (b) potentials.

FF shows a better correlation with the experimental data than that of the PMM model, although the high nonlinearity of the experimental results could not be exactly reproduced by either of the potentials. BKS-predicted volumes are within 3−5% of the experimental values in the range of 300−800 K, with larger deviation at higher temperatures, whereas the PMM deviation in cell volumes is between 6 and 7%.

The experimental volume of the all-silica zeolite SSZ-73 at normal conditions is 2026.5 Å$^3$.[16] We have obtained values of 2119 and 2140 Å$^3$ at 300 K for BKS and PMM potentials, respectively, which are within 5−6% accuracy with respect to the experimental value.[16] BKS gives a closer approximation to the experimental volume and also predicts a steeper negative change in volume with temperature compared to PMM. However, to date no experimental volume variation with temperature for this structure has been reported, so comparison with data at higher temperatures is not possible. Calculated and experimental lattice parameters for the models are presented as Supporting Information.

The Si-CHA window oxygen−oxygen PDFs at 300, 600, and 800 K obtained from NVE MD trajectories using the BKS and PMM FFs are depicted in Figure 3. The BKS effective O−O distances found at 300 K ($D_1$ = 3.83 Å, $D_2$ = 4.20 Å) are slightly larger than the values reported at 300 K by Hedin et al. ($D_1$ = 3.70 Å and $D_1$ = 4.17 Å).[23] This small difference with the experimental results is due to the larger cell volume predicted by the FF.

The peaks in Figure 3a show that average window O−O distances decrease with increasing temperature, which was expected from the cell volume negative thermal behavior predicted; however, the distance changes in a nonsymmetrical way, the variation of $D_2$ being more marked. This unsymmetrical variation has the effect of making the window geometry less elongated. The thermal increase of the O−O distance fluctuations shows that the window opening widens considerably at higher temperatures. This window breathing effect will add to the thermally increased mobility of the guest molecules and therefore will affect the diffusion dynamics.

Figure 3b shows PDFs obtained with trajectories coming from the PMM FF for the Si-CHA framework. The calculated O−O distances at 300 K, $D_1$ = 3.96 Å and $D_2$ = 4.12 Å, are not as close to the experimental values as those predicted by the BKS FF; $D_1$ is actually larger, and $D_2$ is slightly shorter. The window size fluctuations follow a rising pattern with temperature, showing an expanding distribution of the window opening of the same sort as that previously obtained with the BKS FF. The slightly larger window sizes calculated in the range of temperatures with the PMM FF will show up later, allowing a less constrained intercage motion of the guest molecules and therefore producing somewhat larger values of diffusivity.

Likewise, window oxygen−oxygen PDFs for Si-SAS at 300, 600, and 800 K obtained from NVE MD runs using the BKS and PMM potentials are drawn in Figure 4. The effective O−O distances obtained at 300 K with the BKS potential ($D_1$ = 4.24 Å, $D_2$ = 4.26 Å) are comparable to those obtained from the PMM model at 300 K ($D_1$ = 4.24 Å and $D_2$ = 4.28 Å), and a further increase in temperature does not change the picture in a dramatic way. The $D_1$ and $D_2$ values obtained with the experimentally reported data for Si-SAS are $D_1 = D_2$ = 4.25 Å. Again the BKS model predicts more correctly the window size, although for this structure the differences are less pronounced. The same trend found for Si-CHA is obtained for the Si-SAS structure, that is, slightly larger volumes corresponding to larger values of window O−O PDFs predicted with the PMM potential. Both models predict a negative expansion

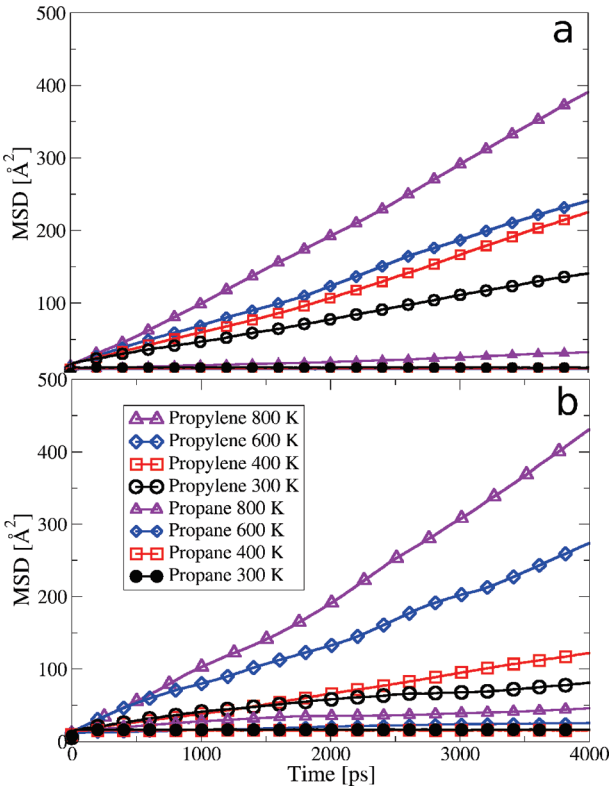


**Figure 5.** MSDs for propane/propylene in Si-CHA from MD trajectories calculated with the BKS (a) and PMM (b) FFs at 300, 600, 400, and 800 K. The loading is set to 0.5 molecule per unit cell.

coefficient for the models, although the temperature dependence of volume for Si-SAS cannot be confirmed with experimental data.

The main difference between O−O PDFs obtained with the different FFs is that although both FFs predict correctly structures with different $D_1$ and $D_2$ window openings, the BKS FF values are in closer agreement to the experimental values. The less pronounced thermal volume variation calculated with PMM is responsible for the almost negligible temperature variations of $D_1$ and $D_2$ in Si-CHA, as we can see in Figure 4b. The same type of thermal window fluctuation is observed with both FFs, that is, a wider and non-negligible fluctuation of window opening parameters $D_1$ and $D_2$ with increasing temperature. The full set of calculated values for the effective window O−O PDFs and corresponding deviations can be seen in the Supporting Information (Tables 2 and 3).

**Propane/Propylene Diffusion.** The diffusion coefficient of adsorbed molecules in a microporous material is a measurement of the time-dependent evolution of the 3-dimensional position of the adsorbate inside the crystalline host structure. From MD simulations we can obtain the self-diffusion coefficient by calculating the MSD of the guest particles as a function of time. We analyze the self-diffusion coefficients obtained from trajectories of propane/propylene adsorbed in Si-CHA/Si-SAS zeolites using the BKS and PMM FFs. Einstein's self-diffusion coefficients for propane and propylene in Si-CHA were calculated from MD trajectories simulated by using the BKS and PMM potentials. The MSDs of propane/propylene at four temperatures (300, 400, 600, and 800 K) are depicted in Figure 5.

Long MD simulations of up to 15 ns were performed to obtain good-quality diffusion coefficients by using a sampling rate of 0.5 ps. These long simulation runs were necessary due to the fact that propane/propylene kinetic diameters are very close to the size of the cages interconnecting 8-MR windows; thus, the intercage motion is quite slow and based on jumps occurring after relatively long intracage residence times. The propane/propylene kinetic diameters measured using the approach developed by Rohrbaugh and Jurs[24] are shown in Table 3 and Figure 6.

**TABLE 3: $L_x$, $L_y$, and $L_z$ Refer to the Lengths of the Shadows Resulting from the Projection of the Molecules with Respect to the Planes *xz*, *xy*, and *yz*, Respectively[24]**

| | shadow lengths (Å) | | |
|---|---|---|---|
| structure | $L_x$ | $L_y$ | $L_z$ |
| propane | 6.72 | 4.59 | 4.21 |
| propylene | 6.67 | 5.28 | 4.21 |
| ethane | 4.937 | 4.32 | 4.43 |
| ethylene | 4.887 | 4.27 | 3.40 |

The so-called "window effect" was experimentally documented for 8-MR structures in the work of Hedin et al.[23] They used a PFG NMR technique to calculate the self-diffusion coefficients of methane, ethylene, ethane, and propylene adsorbed in three siliceous zeolites: DDR, CHA, and LTA. The calculated diffusion coefficients decreased as a function of the increasing size of the guest for a given framework, but for a given adsorbate the coefficient changed according to the size of the 8-MR window. They found that propylene diffusion was only measurable under the experimental conditions for Si-LTA, the material with larger window size, and thus, its diffusional behavior was ascribed to be predominantly affected by the framework window size.

We can see in Figure 5 that the diffusion of propane is extremely slow. At the lower temperatures of 300 and 400 K diffusion coefficients cannot be calculated because the standard error of the MSD slope obtained is, respectively, 2 orders and 1 order of magnitude higher than the slope itself. Thus, we pushed thermal conditions up to the higher simulation temperatures of 600 and 800 K, where there is finally some increase of intercage propane mobility, which allowed the calculation of MSD slopes with lower statistical uncertainty. The standard error of the MSD slope at 600 K is on the same order as the slope. At 800 K this error is 3 orders of magnitude smaller than the calculated diffusional constant, although the intercage mobility is still slow, as can be realized from the scale of the MSD in Figure 5. The intercage motion of the adsorbates only goes as far as the length of one cage-to-cage distance.

Diffusion coefficients calculated for propylene show a higher rate of intercage motion compared to those of propane. The diffusional coefficients calculated with the BKS FF for propylene are in the range $10^{-7}-10^{-6}$ cm$^2$/s for the temperature range

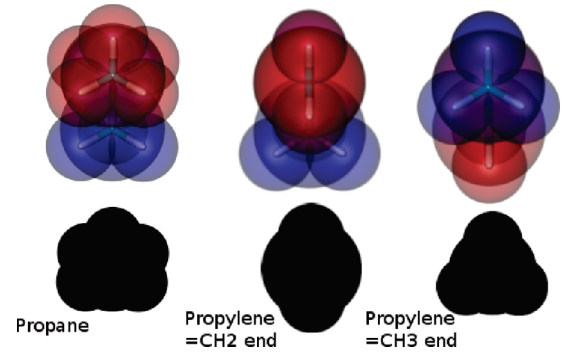


**Figure 6.** Propane and propylene representations and shadows of the terminal $CH_3$ and $CH_2$ ends.

300−800 K. The trends observed for propylene are those expected, with diffusion coefficients several orders of magnitude larger than those obtained for propane: $D_{propylene} \approx 10^{-7}/D_{propane} \approx 10^{-10}$ for the lower 300 K temperature and $D_{propylene} \approx 10^{-6}/D_{propane} \approx 10^{-8}$ at the higher temperature of 800 K. Also, the increasing trend of diffusion coefficients with temperature was expected, as diffusion can be described as an energy-activated process.

The calculated coefficients obtained when using the PMM FF are of about the same order of magnitude as those calculated using the BKS FF for both of the adsorbates in the temperature range considered, although a slight increase in self-diffusion coefficients is seen for the systems simulated at higher temperatures with the PMM FF, as can be observed by comparing parts a and b in Figure 5. The impact of the FF on the diffusion of propane at the lower temperatures of 300 and 400 K cannot be quantified in terms of diffusion coefficients, due to the almost negligible intercage motion of the adsorbate. At 600 K, the slope of the MSD obtained with the PMM FF shows a small but positive value, whereas the slope of the MSD calculated with the BKS potential is totally flat. The diffusion coefficients calculated at this temperature show a difference of about 2 orders of magnitude [$D^{BKS\text{-}600}_{propane} \approx 10^{-6}/D^{PMM\text{-}600}_{propane} \approx 10^{-8}$], although the statistical accuracy of these coefficients is of about the same order of magnitude as the values. Diffusion constants calculated at 800 K show the same order of magnitude, although the value calculated with the PMM model is twice the value obtained with BKS. Thus, the predicted dimensions $D_1$ and $D_2$ of the windows obtained with the different FFs do have a visible impact in diffusion at high temperatures, where the thermally accelerated intercage motion of the adsorbate allows the calculation of statistically meaningful self-diffusion coefficients.

A further testing of the temperature and FF influence on the diffusional behavior of propane/propylene was carried out by simulating the dynamics of these adsorbates in Si-SAS zeolite. Figure 7 shows the MSDs obtained using the BKS and PMM potentials. Self-diffusion coefficients calculated for propylene/propane are presented in Table 4.

As in the case of Si-CHA, the main difference between the FFs is the ability of BKS to model more accurately the structural features of the Si-SAS framework, although for this structure the differences are less marked. Diffusional coefficients obtained with the PMM FF are on about the same order as those coming from the BKS potential, as we can see in Table 4. A salient feature of propylene diffusion when adsorbed in Si-SAS is that although the calculated Si-SAS window size is larger than that of Si-CHA, the self-diffusion coefficient is somewhat smaller compared to the diffusion in Si-CHA. This behavior could be ascribed to the dimensionality of the framework, which is 3-dimensional in Si-CHA and 1-dimensional in Si-SAS; hence, there are more accessible sites to jump in Si-CHA than in Si-SAS where all motion has to occur only in one direction. The order of magnitude of the diffusional coefficients agrees with those calculated with the BKS potential, showing that propylene adsorbed in a Si-SAS framework diffuses slowly, making it necessary to stimulate the systems by raising the temperature to activate the diffusional motion of the adsorbate. The propane diffusion is slower as well, compared with propane diffusing in Si-CHA, and no meaningful diffusional constants could be estimated from the MSDs obtained.

The propylene self-diffusivity follows an Arrhenius-like temperature dependence, as can be expected for a system where intercage guest motion is energy activated. On the other hand, propane diffusion activation energies cannot be calculated from

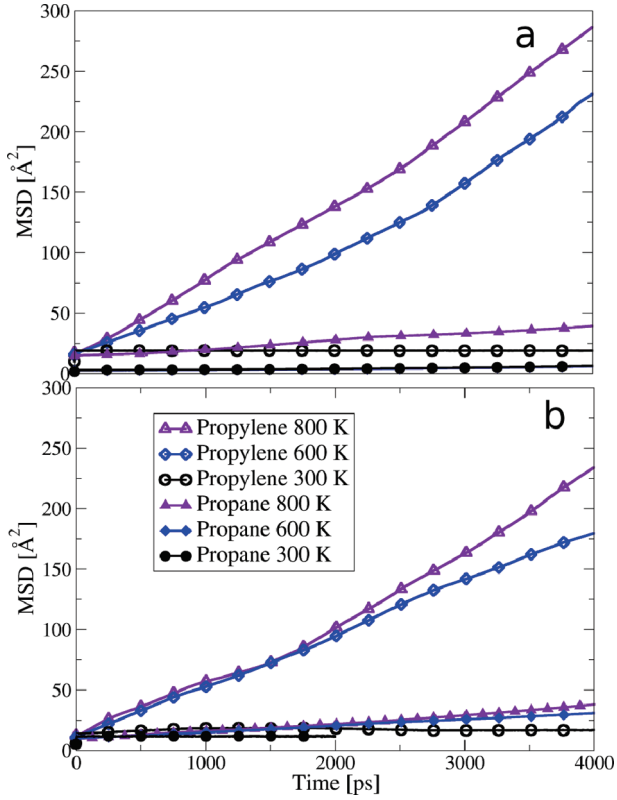


**Figure 7.** MSD for propylene/propane in Si-SAS from MD trajectories calculated with the BKS (a) and PMM (b) FFs at 300, 600, and 800 K.

the available information due to the low level of statistical accuracy of self-diffusivities calculated in the temperature range sampled, which comes as a consequence of the extremely low molecular mobility of the adsorbates. Thus, we have estimated the approximated activation energy for propylene adsorbed in Si-CHA using the higher temperature data of 600 and 800 K. We have to stress here that these results must be seen purely as crudely estimated values because of the high level of statistical uncertainty. The results are presented in Table 5.

As a confirmation of the magnitude of the obtained activation energy, we have calculated the window-crossing energy for propylene and propane in Si-CHA at 800 K following the intermolecular (host−guest) component of the FF. The energy trajectory for propane and propylene in Si-CHA is drawn in Figures 8 and 9 with a maximum occurring at the intermolecular portion of the potential surface corresponding to the point where the guest is just crossing the window.

The calculated energy difference between the peak intermolecular energy and the average is about 5.3 kcal/mol for the case of propylene−Si-CHA, which is several times higher than the activation energy of 1.0−2.3 kcal/mol obtained from the estimated self-diffusional constants. This energy difference is indicative of the underestimation of diffusional coefficients calculated with the MSDs obtained from long trajectories of classical MD trajectories. However, the order of magnitude of the activation energy is on the same order, which gives some confidence about the range of the calculated self-diffusion constants. For the case of propane−Si-CHA, the energy difference between the average energy baseline and the window-crossing event is about 9.0 kcal/mol, almost twice the energy difference for propylene−Si-CHA. The difference in energy for the intercage motion of propylene and propane is a confirmation of the energetic barrier that the guest has to overcome, being almost twice larger for propane.

**TABLE 4: Calculated Self-Diffusion Constants for Propene and Propylene at 600 and 800 K Using the BKS and PMM FFs[a]**

| | $D_{BKS}$ (cm$^2$/s) | | | | $D_{PMM}$ (cm$^2$/s) | | | |
|---|---|---|---|---|---|---|---|---|
| host−guest | 300 K | 400 K | 600 K | 800 K | 300 K | 400 K | 600 K | 800 K |
| CHA−propylene | $5.2 \times 10^{-7}$ | $8.8 \times 10^{-7}$ | $1.0 \times 10^{-6}$ | $1.6 \times 10^{-6}$ | $2.41 \times 10^{-7}$ | $4.6 \times 10^{-7}$ | $1.31 \times 10^{-6}$ | $2.75 \times 10^{-6}$ |
| CHA−propane | $1.0 \times 10^{-10}$ | $1.6 \times 10^{-10}$ | $5.12 \times 10^{-10}$ | $9.6 \times 10^{-8}$ | $1.0 \times 10^{-10}$ | $1.5 \times 10^{-10}$ | $6.0 \times 10^{-8}$ | $1.1 \times 10^{-7}$ |
| SAS−propylene | N/A | N/A | $8.8 \times 10^{-7}$ | $1.1 \times 10^{-6}$ | N/A | N/A | $7.1 \times 10^{-7}$ | $1.1 \times 10^{-6}$ |

[a] Propane diffusion coefficients are tabulated (for Si-CHA) only to show the difficulty of intercage motion; the values calculated cannot be related to the self-diffusion process. Only data for propylene in the SAS framework type at high temperatures are given, as the low-temperature motion is extremely slow.

**TABLE 5: Calculated Self-Diffusion Constant and Arrhenius Activation Energy**

| host−guest | $E_a^{BKS}$ (kcal/mol) | $E_a^{PMM}$ (kcal/mol) |
|---|---|---|
| CHA−propylene | 1.0 | 2.3 |

## Conclusion

Zeolites with narrow eight-membered oxygen rings have been recognized as good candidates for separations of olefin/paraffin mixtures based on molecular sieving effects. From experimentally synthesized pure silica 8-MR structures and experimental diffusion studies it is possible to conclude that small differences in window size make a big difference for intracrystalline motion.[23] In this work we have studied the temperature effects on window sizes of two pure silica eight-membered ring framework types: Si-CHA and Si-SAS. The framework negative volume variation with temperature was taken into account by simulating the frameworks in the NPT ensemble and allowing enough simulation time for volume equilibration at the target temperature. From the average value of the volume obtained in this way, initial configurations for MD simulations in the NVE ensemble were generated. The BKS potential predicted Si-CHA volumes with higher accuracy than those predicted with the PMM model. Also, the change of volume for Si-CHA with temperature was best described by the BKS model, although none of the potentials could describe accurately the high nonlinearity of this property. The window size of Si-CHA and Si-SAS and temperature fluctuations were obtained from PDFs with MD-NVE simulations including full flexibility of the framework. The window size widens considerably at higher temperatures, thus providing a lower barrier to diffusion. Also, the temperature-activated mobility of the guest molecules helps to overcome the cage-to-cage energy barrier, raising the frequency of intercage jumps.

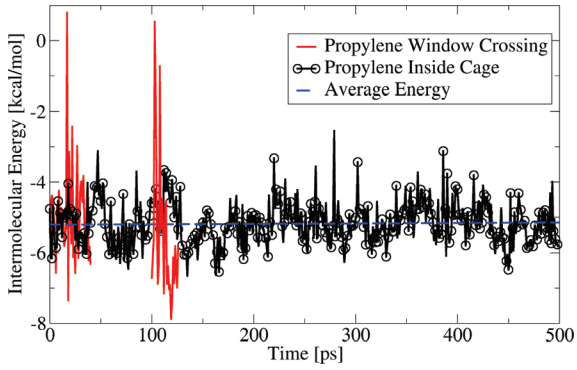


**Figure 8.** Intermolecular component of the potential energy from a trajectory showing two window-crossing events represented in red. All trajectories were obtained from simulated propylene adsorbed in Si-CHA with the BKS model at 800 K. The average energy of a propylene molecule while trapped in a cage is shown as the noncontinuous blue line. The host−guest intermolecular energy for a 500 ps trajectory is shown in black and corresponds to the intracage motion of the guest without crossing the window.

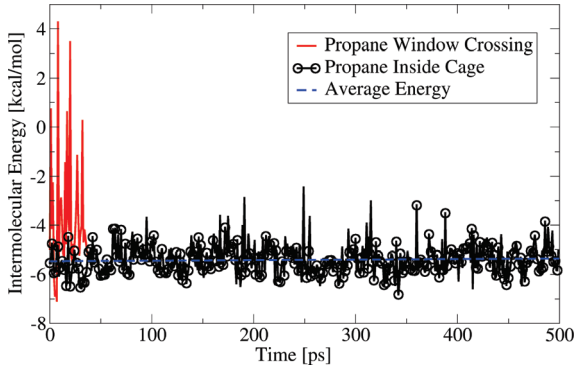


**Figure 9.** Intermolecular component of the potential energy from a trajectory showing two window-crossing events represented in red. All trajectories were obtained from simulated propane adsorbed in Si-CHA with the BKS model at 800 K. The average energy of a propane molecule while trapped in a cage is shown as the noncontinuous blue line. The host−guest intermolecular energy for a 500 ps trajectory is shown in black and corresponds to the intracage motion of the guest without crossing the window.

Thermal influence on diffusional coefficients of propane/propylene molecules adsorbed in Si-CHA and Si-SAS zeolites was obtained from equilibrium MD simulations in the NVE ensemble. Potential energy surface effects were taken into account by comparing the results from the well-known BKS potential and the PMM potential. The PMM potential, which predicts a wider window size for the structures chosen, also predicts slightly larger self-diffusional constants in all cases. However, the low intercage mobility of either propane or propylene at low temperatures forbids the calculation of statistically meaningful diffusional coefficients. The high-temperature estimated self-diffusional constants for propylene in Si-CHA were used to calculate the activation energy. It has to be stressed that the so-calculated activation energy only represents a crude estimation and is only useful for a general comparison with the intermolecular portion of the potential energy surface. The intermolecular energy calculated from NVE trajectories for the window-crossing events was almost 2 times larger for propane than for propylene in Si-CHA, confirming the difference in activated diffusional motion between guests. Also, the activation energy calculated from the self-diffusional constants was several times shorter than that coming from the host−guest potential, which clearly indicates an underestimation of the self-diffusional constant value. This underestimation arises from the fact that the trajectories simulated do not sample the guest motion far enough, producing a low statistical certainty.

Recent efforts in simulation techniques, computationally less costly, are available to calculate diffusional constants of tight-fitting host−guest systems. Strategies based on the transition-state theory (TST),[25] as well as approaches that take advantage of the thermal activation of molecular motion at high temper-

atures,[26] provide methodologies to predict the diffusional behavior in slowly diffusing host−guest systems. However, some of these models are used on the basis of several drastic assumptions, the fixed framework assumption possibly being the most influential one. Criticisms of this type of approximation have been made recently, especially regarding the use of fixed framework approaches at high temperatures, where the dynamics of the host is critical and even more influential for slowly diffusing guests.[27] We will make use of some of the TST-based approaches in the future, including flexibility of the framework and a correct treatment of the vibrational modes, to estimate the magnitude of sorption and diffusional features of host−guest systems in a statistically more meaningful way.

**Acknowledgment.** Funding through the Ministerio de Ciencia e Innovaci and computing time from Red Espa are acknowledged. A.F.C. thanks the Instituto de Tecnología Química, UPV-CSIC, for providing a research fellowship.

**Supporting Information Available:** S-SAS and Si-CCHA calculated and experimental lattice parameters, Si-CHA calculated and experimental volume and window size data, and Si-SAS calculated and experimental volume and window size data. This material is available free of charge via the Internet at http://pubs.acs.org.

## References and Notes

(1) Corma, A. *J. Catal.* **2003**, *216*, 298–312.
(2) Song, L.; Sun, Z.; Duan, L.; Gui, J.; McDougall, G. S. *Microporous Mesoporous Mater.* **2007**, *104*, 115–128.
(3) Li, Z.; Johnson, M. C.; Sun, M.; Ryan, E. T.; Earl, D. J.; Maichen, W.; Martin, J. I.; Li, S.; Lew, C. M.; Wang, J.; Deem, M. W.; Davis, M. E.; Yan, Y. *Angew. Chem., Int. Ed.* **2006**, *45*, 6329–6332.
(4) Keller, G. E.; Marcinkowsky, A. E.; Verma, S. K.; Williamson, K. D. *Separation and Purification Technology*; Marcel Dekker: New York, 1992.
(5) Kärger, J.; Ruthven, D. M. *Diffusion in Zeolites and Other Microporous Solids*; John Wiley and Sons: New York, 1992.
(6) Ruthven, D. M. *Principles of Adsorption and Adsorption Processes*; Wiley-Interscience: New York, 1984.
(7) Palomino, M.; Cantín, A.; Corma, A.; Leiva, S.; Rey, F.; Valencia, S. *Chem. Commun.* **2007**, 1233–1235.
(8) ter Horst, J. H.; Bromley, S. T.; van Rosmalen, G. M.; Jansen, J. C. *Microporous Mesoporous Mater.* **2002**, *53*, 45–57.
(9) Demontis, P.; Suffritti, G. B. *Chem. Rev.* **1997**, *97*, 2845–2878.
(10) Auerbach, S. M.; Jousse, F.; Vercauteren, D. P. Dynamics of Sorbed Molecules in Zeolites. *Computer Modelling of Microporous and Mesoporous Materials*; Academic Press: New York, 2004.
(11) Lightfoot, P.; Woodcock, D. A.; Maple, M. J.; Villaescusa, L. A.; Wright, P. A. *J. Mater. Chem.* **2001**, *11*, 212–216.
(12) Woodcock, D. A.; Ligthfoot, P.; Villaescusa, L. A.; Díaz-Cabañas, M. J.; Camblor, M. A.; Engberg, D. *Chem. Mater.* **1999**, *11*, 2508–2514.
(13) van Beest, B. W. H.; Kramer, G. J.; van Santen, R. A. *Phys. Rev. Lett.* **1990**, *64*, 1955–1958.
(14) Pedone, A.; Malavasi, G.; Menziani, M. C.; Cormack, A. N.; Segre, U. *J. Phys. Chem. B* **2006**, *110*, 11780–11795.
(15) Herzbach, D.; Binder, K.; Müser, M. H. *J. Chem. Phys.* **2005**, *123*, 124711.
(16) Wragg, D. S.; Morris, R.; Burton, A. W.; Zones, S. I.; Ong, K.; Lee, G. *Chem. Mater.* **2007**, *19*, 3924–3932.
(17) Díaz-Cabañas, M. J.; Barrett, P. A.; Camblor, M. A. *Chem. Commun.* **1998**, 1882–1882.
(18) Smith, W.; Yong, C. W.; Rodger, P. M. *Mol. Simul.* **2002**, *28*, 385–471.
(19) Ewald, P. P. *Ann. Phys.* **1921**, *64*, 253.
(20) Oie, T.; Maggiora, T. M.; Christopherssen, R.; Duchamp, D. J. *Int. J. Quantum Chem., Quantum Biol. Symp.* **1981**, *8*, 1.
(21) Catlow, C. R. A.; Freeman, C. M.; Vessal, B.; Tomlinson, S. M.; Leslie, M. *J. Chem. Soc., Faraday Trans.* **1991**, *87*, 1947.
(22) Llopis, F.; Sastre, G.; Corma, A. *J. Catal.* **2004**, *227*, 227–241.
(23) Hedin, N.; De Martin, G. J.; Roth, W. J.; Strohmaier, K. G.; Reyes, S. A. C. *Microporous Mesoporous Mater.* **2008**, *109*, 327–334.
(24) Rohrbaugh, R. H.; Jurs, P. *Anal. Chim. Acta* **1987**, *199*, 99–109.
(25) Beerdsen, E.; Smit, B.; Dubbeldam, D. *Phys. Rev. Lett.* **2004**, *93*, 248301.
(26) Nagumo, R.; Takaba, H.; Nakao, S.-i. *J. Phys. Chem. B* **2003**, *107*, 14422–14428.
(27) Demontis, P.; Suffritti, G. B.; Yashonath, S. *J. Phys. Chem. C* **2008**, *112*, 17030–17031.

JP903245J